Neuroscience 116 (2003) 201–211

HIPPOCAMPAL NETWORK PATTERNS OF ACTIVITY IN THE MOUSE

G. BUZSÁKI,[a]* D. L. BUHL,[a] K. D. HARRIS,[a] J. CSICSVARI,[a] B. CZÉH[a] AND A. MOROZOV[b]

[a]*Center for Molecular and Behavioral Neuroscience, Rutgers, The State University of New Jersey, 197 University Avenue, Newark, NJ 07102, USA*

[b]*Center for Neurobiology and Behavior College of Physicians and Surgeons, Columbia University, New York, NY 10032, USA*

Abstract—Genetic engineering of the mouse brain allows investigators to address novel hypotheses *in vivo*. Because of the paucity of information on the network patterns of the mouse hippocampus, we investigated the electrical patterns in the behaving animal using multisite silicon probes and wire tetrodes. Theta (6–9 Hz) and gamma (40–100 Hz) oscillations were present during exploration and rapid eye movement sleep. Gamma power and theta power were comodulated and gamma power varied as a function of the theta cycle. Pyramidal cells and putative interneurons were phase-locked to theta oscillations. During immobility, consummatory behaviors and slow-wave sleep, sharp waves were present in cornu ammonis region CA1 of the hippocampus stratum radiatum associated with 140–200-Hz "ripples" in the pyramidal cell layer and population burst of CA1 neurons. In the hilus, large-amplitude "dentate spikes" occurred in association with increased discharge of hilar neurons. The amplitude of field patterns was larger in the mouse than in the rat, likely reflecting the higher neuron density in a smaller brain. We suggest that the main hippocampal network patterns are mediated by similar pathways and mechanisms in mouse and rat.

Key words: EEG, pyramidal cells, theta, gamma, ripples, transgenic.

Collective behavior of neurons offers a link between complex behaviors governed by the brain and biophysical, synaptic properties of individual neurons. Coherent membrane currents, brought about by synaptic activity and intrinsic properties of neurons, pass through the extracellular space and can be measured by electrodes placed outside the neurons as local field potentials. Together with extracellular monitoring of single-cell outputs, local field potentials provide an insight into the cooperative properties of neuronal networks (Buzsáki, 2002). In the rat hippocampus, the most characteristic collective patterns are oscillations in the theta (6–10 Hz), gamma (~40–100 Hz) and ultra-fast (140–200 Hz) bands (cf. Buzsáki et al., 1994; Jefferys et al., 1996; Leung, 1998; Bland and Oddie, 2001). To date, most knowledge regarding the cellular-synaptic mechanism of hippocampal oscillations and their behavioral relevance derives from studies in the rat (cf. Stewart and Fox, 1990; Vertes and Kocsis, 1997; Bland and Oddie, 2001; Buzsáki, 2002).

Theta and gamma oscillations in the hippocampal system arise from a consortium of coupled oscillators and resonators. Theta waves depend on ongoing behavior (Grastyán et al., 1959; Vanderwolf, 1969; Stumpf, 1965). Theta oscillations are most consistently present during rapid eye movement (REM) sleep (Jouvet, 1969) and during various types of locomotor activities described by the psychological terms *voluntary*, *preparatory*, *orienting* or *exploratory* (Vanderwolf, 1969). Gamma waves are nested on the slower theta oscillation (Bragin et al., 1995a). In the absence of theta rhythm, the power and regularity of gamma oscillation decreases and different irregular patterns appear (Vanderwolf, 1969). Sharp waves in the cornu ammonis regions CA1 and CA3 of the hippocampus (CA1, CA3) stratum radiatum reflect transient depolarization of pyramidal cell dendrites by the synchronously discharging CA3 network (Buzsáki et al., 1983; Csicsvari et al., 2000). Concurrent with the slow dendritic sharp wave event, a short-lived ultra-fast oscillation ("ripple") is present in the CA1 pyramidal layer (O'Keefe and Nadel, 1978; Buzsáki et al., 1992). Another irregular pattern emerges in the dentate hilus, termed "dentate spike" (Bragin et al., 1995b). Dentate spikes are associated with the synchronous discharge of granule cells and interneurons. The likely triggers of dentate spikes are population bursts in the basolateral amygdala (Paré et al., 1995). Sharp waves and dentate spikes are present during immobility, consummatory behaviors and slow-wave sleep.

Although proper synaptic connectivity among neuronal networks is essential for population rhythms, intrinsic membrane properties of hippocampal neurons are selectively tuned to resonate at these network frequencies (Llinás, 1988; Alonso and Llinás, 1989; Leung and Yim, 1991; Kamondi et al., 1998; Penttonen et al., 1998; Pike et al., 2000). The power, frequency and spatial coherence of these rhythms and their relationship to timing of action potentials of pyramidal cells and inhibitory interneurons are therefore quantitative phenotypes that may be altered by various manipulations of channel properties and receptors of targeted neuronal populations. Because specific and selective manipulations can be brought about most reliably by genetic engineering in the mouse (e.g. Rotenberg et al., 1996; McHugh et al., 1996; Wilson and Tonegawa, 1997; Joho et al., 1999; Stowers et al., 2002), it is important to understand the nature of these population patterns in the intact mouse.

*Corresponding author. Tel: +1-973-353-1080 ext. 3131; fax: +1-973-353-1820.
E-mail address: buzsaki@axon.rutgers.edu (G. Buzsáki).

Abbreviations: CA1, CA3, cornu ammonis regions of the hippocampus; DS, dentate field spike; EEG, electroencephalogram; REM, rapid eye movement.

0306-4522/03$30.00+0.00
PII: S0306-4522(02)00669-3

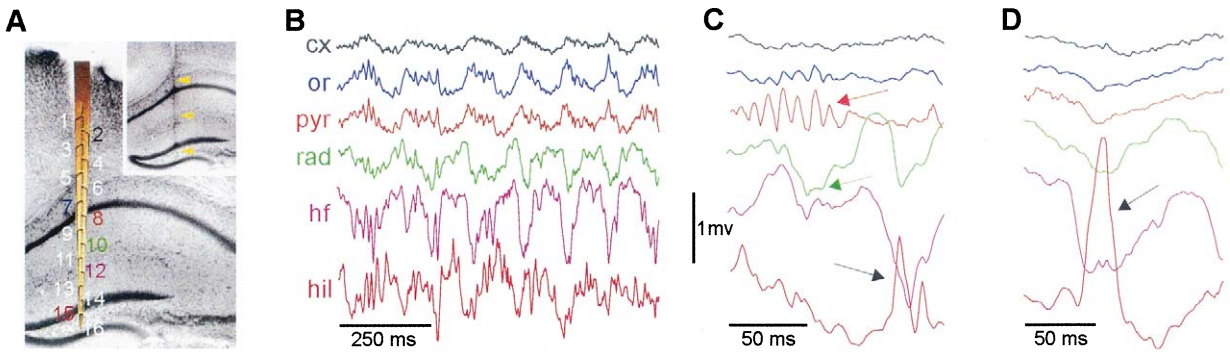

Fig. 1. Voltage-versus-depth profile of hippocampal field activity in the mouse. (A) Location of a 16-site silicon probe in the CA1–dentate gyrus axis. Numbers indicate recording sites (100-μm spacing). Inset, arrowheads indicate the probe track. (B) Theta–gamma oscillation recorded during wheel running. Color-coded traces correspond to locations in A (cx, neocortex; or, stratum oriens; pyr, pyramidal layer; rad, stratum radiatum; hf, hippocampal fissure; hil, hilus). (C) Fast field oscillation ("ripple," red arrow) in the pyramidal cell layer associated with a negative sharp wave in stratum radiatum (green arrow). A DS with polarity reversal across the dentate granule cell layer is also shown (black arrow). (D) DS in isolation.

In contrast to the rat, local field and/or unit recording studies in the behaving mouse are rare (Jaffard and Jeantet, 1981; Destrade, 1982; Glinn et al., 1990; Kasamo et al., 1992; Toth et al., 1995; McHugh et al., 1996; Rotenberg et al., 1996; Noebels, 1996; Joho et al., 1999; Kim et al., 2001; Ikonen and Tanila, 2001; Hajdu et al., 2002). The present study was undertaken to examine population patterns in the hippocampus of the mouse.

EXPERIMENTAL PROCEDURES

Surgery and recording

Thirteen male progeny of C57B6/J (Jackson Laboratories, Bar Harbor, ME, USA) and 129S6/SvEvTac (Taconic Farms, Germantown, NY, USA) hybrid mice and three C57B6/J inbred mice (Jackson Laboratories) were anesthetized with a mixture of (4 ml/kg) of ketamine (25 mg/ml), xylazine (1.3 mg/ml), and acepromazine (0.25 mg/ml) via an i.m. injection (25–35 g; 3–6 months old). To record field potential and unit activity, the mice were chronically implanted with a microdrive that allowed the movement of two to eight recording electrodes in the same or opposite hemispheres. Two holes (approximately 1 mm in diameter) were drilled bilaterally 1.7 mm posterior to bregma and ±1.0 mm lateral to the midline. The electrodes were either single wires (60-μm diameter) or composed of four individually insulated nichrome wires (13-μm diameter). The wires were twisted, gold-plated to reduce impedance (200–400 kohm at 1 kHz) and fused to form a "tetrode" (Gray et al., 1995). During surgery the electrodes were placed in the shallow layers of the isocortex and the hole was covered with a mixture of paraffin oil and wax. After the electrodes were in position, the microdrive was fixed to the skull with dental acrylic. Each complete turn of the microdrive moved the recording electrode ~0.3 mm axially. In four mice, a 16-site silicon probe was implanted into the right hippocampus (Fig. 1A; Bragin et al., 1995a). The distance between the recording sites (108 μm) was 100 μm. Two stainless steel screws were driven into the skull above the frontal cortex and served as ground and reference electrodes. Two additional screws were implanted posterior to lambda to serve as anchors. Each mouse was then placed one to a cage where food and a dish of water were placed on the floor of the cage for easy access. For comparison with physiological data in the rat, data from four adult male Sprague–Dawley rats (300–400 g) were used (Czurkó et al., 1999). Care was taken to minimize the suffering of the animals, and all procedures conformed to the National Institutes of Health Guide for the Care and Use of Laboratory Animals and had been approved by the Institutional Animal Care and Use Committee, Rutgers University. The use of multiple site electrodes reduced the number of mice needed.

Recording and data processing

Unit and field activities were recorded in either the home cage or a wheel running apparatus. The latter consisted of a running wheel (29.5 cm in diameter) and adjacent box (30 cm×40 cm×35 cm; Czurkó et al., 1999). The mice were allowed to freely explore the apparatus and run in the wheel. Instrumentation amplifiers, built in the female connector (16 channels), were used to reduce cable movement artifacts. Field potential and unit activity were recorded after being amplified (2000–5000×) and band-pass filtered (1 Hz–3 kHz; Grass Instruments, Quincy, MA, USA), digitized with 12-bit resolution continuously at 10–20 kHz (ISC-16 analog-to-digital converter; RC Electronics, Santa Barbara, CA, USA), and recorded on a personal computer. The data were then stored on a separate computer and analyzed off-line. The tetrodes were lowered slowly into the CA1 region of the hippocampus and eventually to the dentate gyrus. For orientation during recording, the position of the electrode in the CA1 pyramidal layer was provisionally determined by the presence of fast field oscillations ("ripples") and associated neuronal firing of CA1 pyramidal cells and interneurons (Buzsáki et al., 1992) and later verified histologically. Recordings from the hilus were characterized by large-amplitude gamma waves during exploration and field "dentate spikes" during immobility (Bragin et al., 1995a,b).

Spike sorting

Putative single units were separated as described by Csicsvari et al. (1999a,b) and Harris et al. (2000). In short, the continuously recorded wide-band signals were high-pass filtered (0.8–5 kHz) digitally. The power (root mean square) of the filtered signal was computed in a sliding window (0.2 ms) for spike detection. Spikes with power of more than five times the S.D. from the baseline mean were extracted. The spike waveforms were reconstructed to 40 kHz by using the sampling theorem (Csicsvari et al., 1999a,b), and the peaks of the original and reconstructed waveforms were realigned. Principal component analysis was used to extract features from the wave shapes. The first three principal components were calculated for each channel recorded by the electrode. Units were identified and isolated by using an auto-clustering method followed by manual adjustment (Csicsvari et al., 1999a,b; Harris et al., 2000). Three independent criteria were used to separate interneurons from pyramidal cells: discharge frequency, spike du-

ration and discharge dynamics as measured by the first moment of the autocorrelogram (Csicsvari et al., 1999a,b). Units that could not be clearly isolated and units recorded from single 60-μm wire electrodes were grouped as multiple unit activity.

Detection of ripple, theta and gamma events

For electroencephalogram (EEG) analysis, the data were digitally resampled to 1.25 kHz and then filtered for theta (4–12 Hz), gamma (30–80 Hz), or ripples (150–250 Hz) using a Hamming window-based FIR filter (filter orders 200, 400, and 30, respectively). For the extraction of the ripple events, the power (root mean square) of the band-pass filtered field was quantified and the beginning, peak and end of individual ripple episodes were calculated (Csicsvari et al., 1999a,b). Epochs >7 S.D. of the background mean were classified as ripple episodes. The troughs of individual ripple waves were then detected by finding the minimum points during each episode. Power spectra for individual ripple events were computed using the multi-taper method (window size=1024, [NW]=1.5). Hippocampal theta epochs were automatically identified by using the theta/delta power ratio (Csicsvari et al., 1998) and only periods of 15 seconds or more were used for analysis. Within these periods, instantaneous theta and gamma mean-to-peak amplitudes and phases were extracted by applying Hilbert transform to the previously band-pass filtered EEG. To compute the gamma amplitude as a function of theta phase, the instantaneous gamma amplitude was averaged for every 10° of the theta cycle. Power spectra and coherences were computed using Welch's method and a Hanning window with 512 samples and a 50% overlap. To produce the "Comodugram" (see Figs. 4C, 5B), a multi-taper spectrogram estimate was computed (window size=1024, no overlap, NW=3), and the correlation of log-power was computed for each pair of frequencies.

Histology

Following completion of the experiments, the rats were deeply anesthetized (pentobarbital at 100 mg/kg). With the electrodes left *in situ*, animals were perfused transcardially with saline (~15 ml), followed by 50 ml of phosphate-buffered (0.1-M) fixative (4% paraformaldehyde, 0.15% picric acid, and 0.05% glutaraldehyde). Brains were extracted, blocked within range of the hippocampus, and placed in fixative for 24–48 h. The brains were then cut into 80-μm-thick sections using a vibratome. For verification of electrode placement, sections were mounted onto gelatin-coated slides, stained with the Nissl method, dehydrated and covered with Depex for light microscopy.

RESULTS

Theta oscillations

Depth distribution of theta waves was studied by simultaneous recording of field activity in various hippocampal layers by silicon probes (n=4 mice). Although the spacing of the recording sites (100 μm) did not allow for a detailed analysis of the current sink–source distribution of theta waves in the various hippocampal layers, the depth vs. voltage profiles indicated that theta waves were likely generated by synaptic inputs similar to those in the rat. Theta waves were coherent and in phase above the CA1 pyramidal cell layer and the phase gradually changed in the stratum radiatum, reaching a full reversal (180°) in stratum lacunosum-moleculare (Fig. 1B). The amplitude of theta waves increased gradually from the overlying neocortex to the CA1 pyramidal layer, followed by an amplitude minimum just below the pyramidal layer. The largest-amplitude theta waves (>1 mV) were present at the level of the hippocampal fissure, followed by those in the hilus. However, theta waves in the hilus were superimposed by large-amplitude gamma waves, making the appearance of theta oscillation in this region less striking.

The form of theta waves (wide-band: 1 Hz–3 kHz) was also correlated with the recording depth and deviated from the sinusoid shape considerably at nearly all depths. Theta waves in and above the CA1 pyramidal layer had a sawtooth appearance, with a fast upstroke of positive polarity and a slower downstroke with several gamma waves. In stratum radiatum and lacunosum-moleculare, the fast component was negative and the gamma waves were present mostly on the slow ascending phase. During fast running with increased theta frequency, the asymmetry of the waves increased and the positive component in the pyramidal layer sometimes consisted of only a sharp spike of <40 ms duration (e.g. Figs. 2A, 4A), followed by several gamma cycles on the descending part of the cycle. Theta waves in the hilus were closest to the sinusoid shape, although superimposed by large gamma waves.

The phase relationship between theta oscillation and unit discharge (Fig. 2) is summarized in Fig. 3. The mean firing rates of pyramidal cells was 2.46±0.31 Hz during theta and 2.65±0.25 Hz during non-theta behaviors (i.e. similar to results obtained by McHugh et al., 1996). These averages may overestimate the mean firing rate of all pyramidal neurons because most pyramidal cells discharge at a very low rate (0.1 Hz) and therefore are not detected by the clustering method (Harris et al., 2000). The firing rates of interneurons were 15.32±2.5 Hz and 10.05±1.53 Hz during these respective behaviors. The phase relationship between discharge probability and theta cycle was different for interneurons and pyramidal cells (Fig. 3B, C). Pyramidal neurons had two peaks, one approximately 30° after the trough of theta waves recorded in the pyramidal layer and another maximum at the peak of the theta cycle (Fig. 3C). The double peak was not necessarily due to combining neurons with distinct phase preferences, since double peaks were also observed in theta-phase histograms of individual units. A major source of phase variability was the instant discharge frequency of the neuron. Low-frequency spikes occurred around the peak of CA1 pyramidal layer theta, whereas phase showed a forward shift to the trough at higher frequencies (Harris et al., 2002). Individual interneurons showed a strong theta phase locking and the theta phase relationship showed considerable variability. As a group, they discharged maximally 30–120° prior to the theta trough (Fig. 3B), i.e. on the descending portion of the theta waves.

Gamma oscillations and interaction between theta and gamma waves

In contrast to the rat (Buzsáki et al., 1983; Fig. 4E), gamma waves in the mouse were prominent in the CA1 pyramidal layer (Fig. 4A–D). Individual gamma waves could be resolved by eye. Occasionally, isolated large gamma waves (>0.5 mV) exceeded the amplitude of the carrier theta waves, giving rise to a spikelike appearance (Fig. 4A).

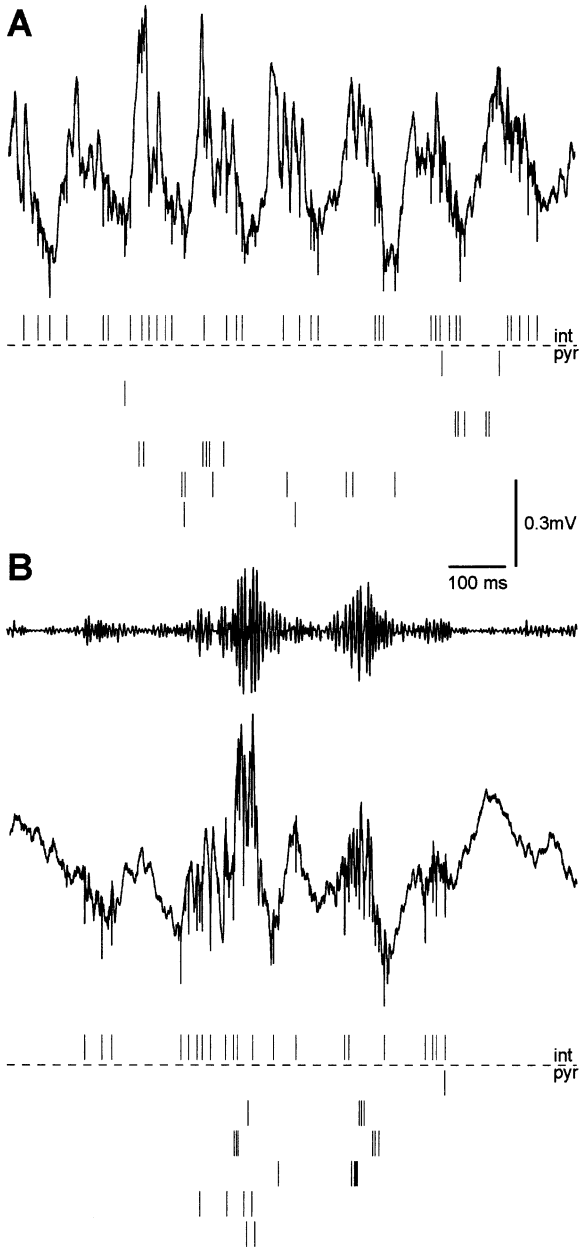

Fig. 2. Parallel-recorded neurons and field in the CA1 pyramidal cell layer during REM sleep and slow-wave sleep (only one site of the tetrode recording is shown). (A) Theta–gamma field activity (1 Hz–3 kHz) and associated action potentials of an isolated interneuron and six pyramidal cells (vertical ticks). Note rhythmic repetition of interneuron discharges at theta frequency. (B) Double sharp wave–associated ripples (top filtered trace; 150–250 Hz). Note clustering of pyramidal cell action potentials during ripples.

Gamma activity was present both during theta- and non-theta-associated behaviors. However, the power and regularity of gamma waves were significantly larger during theta-associated behaviors than during immobility, grooming and slow-wave sleep characterized by non-theta field patterns ($P<0.03$; $t=2.48$; $n=8$; Fig. 4B, D). Because the CA1 pyramidal layer could be reliably identified in every animal, recordings from this layer were used for generating

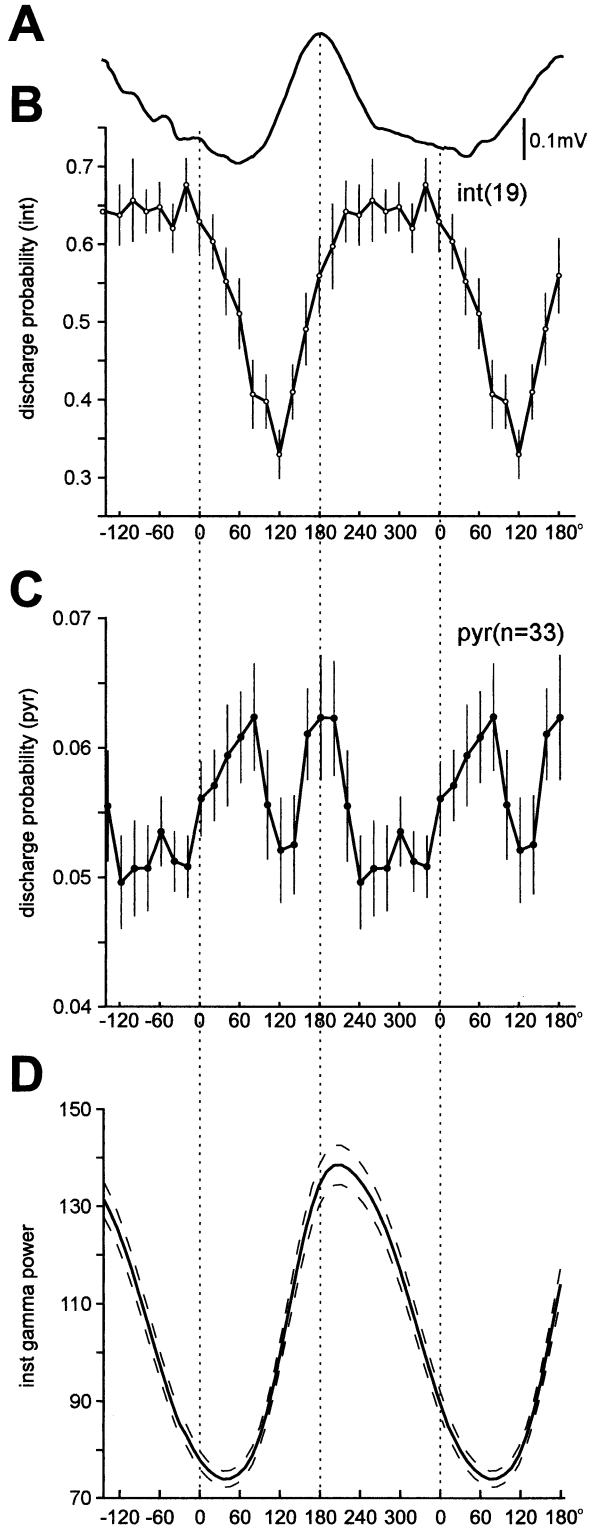

Fig. 3. Theta phase and unit activity. (A) Average theta waves (1 Hz–3 kHz) from a single experiment ($n=>5000$ sweeps; two cycles are shown). (B, C) Discharge probability (±S.E.) of interneurons (B, int) and pyramidal neurons (C, pyr) and as a function of theta cycle. (D) Modulation of gamma power in the cycle. Ordinate, instantaneous gamma power. Largest power of gamma occurs 21.89±0.38° after the theta peak. Averaged data (±S.E.) from 10 mice.

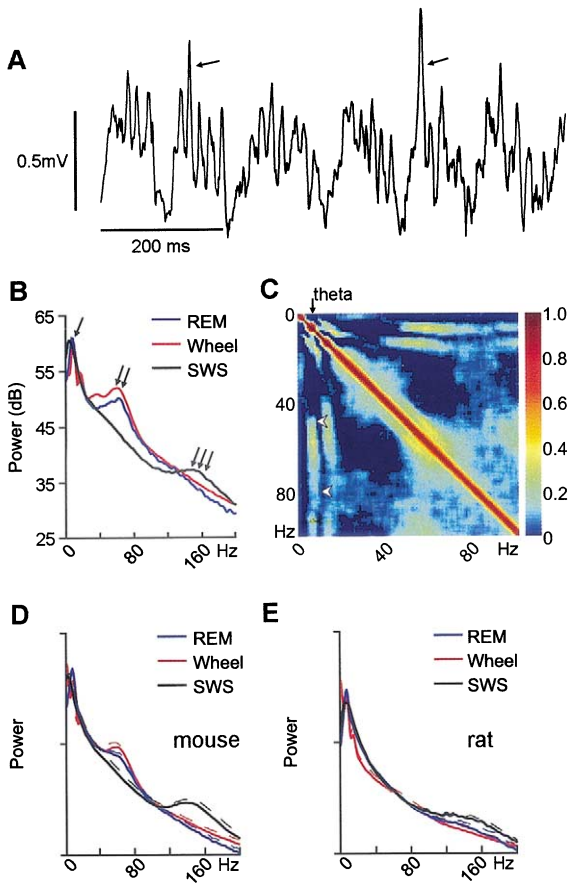

Fig. 4. Relationship between theta and gamma oscillations. (A) Wire tetrode recording from the CA1 pyramidal cell layer. Note large-amplitude gamma oscillations mostly on the positive phase of theta waves. Arrows, large gamma waves (gamma "spikes"). (B) Spectral power (log scale) during wheel running (red), REM sleep (blue) and slow-wave sleep (SWS, black) in a single mouse. Note largest power peak at 8–9 Hz (theta, arrow). A wider peak (40–100 Hz) indicates gamma frequency band (double arrow). Note also increased power at 130–200 Hz during SWS reflecting "ripples" (triple arrow). (C) "Comodugram" showing the correlation between instantaneous theta and gamma power. x- and y-axes, frequency; correlation coefficient (arbitrary units) is color coded. Arrowheads, co-modulation of theta (9 Hz) power and gamma power (50–80 Hz). (D, E) Group data of power in the mouse (n=10) and rat (n=4) during wheel running, REM sleep and slow-wave sleep. Note the larger peaks of power at gamma and ripple frequency in the mouse compared with the rat. Dashed lines: S.E.M. Ordinate: normalized units.

group data. The mean amplitudes of theta and gamma in the pyramidal layer were 336.6±22.98 μV and 175.7±15.88 μV (n=10), respectively. The frequency of gamma activity varied from 40–100 Hz, as shown by a wide peak of power and high coherence values in this frequency band (Figs. 4B, 5C, D).

Theta and gamma oscillations were strongly related in other respects as well. First, we examined common fluctuation in the power of theta and gamma oscillations. In all mice examined, powers of theta and gamma oscillations were correlated, i.e. at times when theta power increased, it was accompanied by an increased power of gamma activity (yellow band at the intersection between 9 Hz and 50–80 Hz in Fig. 4C). In addition, we examined the relationship between instantaneous gamma power and the phase of the theta cycle. These calculations showed that the power of gamma activity fluctuated periodically and reached maximum values at 21.89±0.38° (n=10) after the theta peak recorded in the CA1 pyramidal layer (see Fig. 3D), i.e. coinciding with the maximum discharge probability of the interneurons. When the recording electrode was positioned in stratum radiatum or lacunosum-moleculare, maximum gamma power occurred on the trough or the rising phase of local theta, due to the gradual phase shift of theta (not shown). In other words, the phase relationship between gamma power and theta phase predicted the location of the recording depth.

Bilateral synchrony of theta and gamma oscillations

Bilateral recordings in homologous areas provided signals of similar amplitude, wave shape and phase (Fig. 5). Field recordings from electrodes placed in the left and right CA1 pyramidal layer were highly coherent in the theta and gamma frequency bands (Fig. 5A, D). Coherence values were highest for the theta frequency band (0.89±0.05; n=4) and its harmonics, followed by the gamma frequency band (0.58±0.02). Coherence values above 100 Hz decreased rapidly (<0.2; Fig. 5D). Phase showed little variance (<20°) up to approximately 100 Hz, beyond which the phase fluctuated randomly, indicating insufficient coherence to allow phase measurement. In addition to bilateral similarity of phase in the theta and gamma frequency band, the power modulation of the signals derived from the left and right hippocampi also correlated in these frequency bands (Fig. 5B). During exploration and REM sleep, co-modulation of power was similarly high for theta and gamma oscillations (diagonal in Fig. 5B), with lower values in the intervening frequencies and frequencies above 100 Hz (not shown). In addition, theta power in one hemisphere correlated with gamma power recorded from the contralateral side (arrowhead in Fig. 5B).

Sharp-wave/ripples in the CA1 region

During immobility and slow-wave sleep, the most conspicuous event in the field potential was a fast oscillatory event in the CA1 pyramidal layer (ripple), associated with a negative wave in stratum radiatum (Figs. 1C, 6A, B;O'Keefe and Nadel, 1978; Buzsáki et al., 1992). The magnitude of ripple waves was largest in the middle of the pyramidal cell layer (391.6±2.91 μV; n=14). These ripple events were reflected as increased power in the 120–180-Hz band with a peak at 149.9±1.71 Hz (Figs. 1C, 2B, 6C; McHugh et al., 1996). Ripples occurred relatively irregularly but not randomly. First, ripples often occurred as "doublets," as reflected by a peak at 100–200 ms in the ripple-episode autocorrelogram (Figs. 2B, 6E), due to phase coupling between ripples and neocortical sleep spindles (A. Sirota and G.B., unpublished observations). Second, during slow-wave sleep additional peaks were present at 2–4 and 10–20 s, likely reflecting network excitability changes associated with slow and ultraslow oscillation periods (Steriade et al., 1993; Penttonen et al., 1999; Leinekugel et al.,

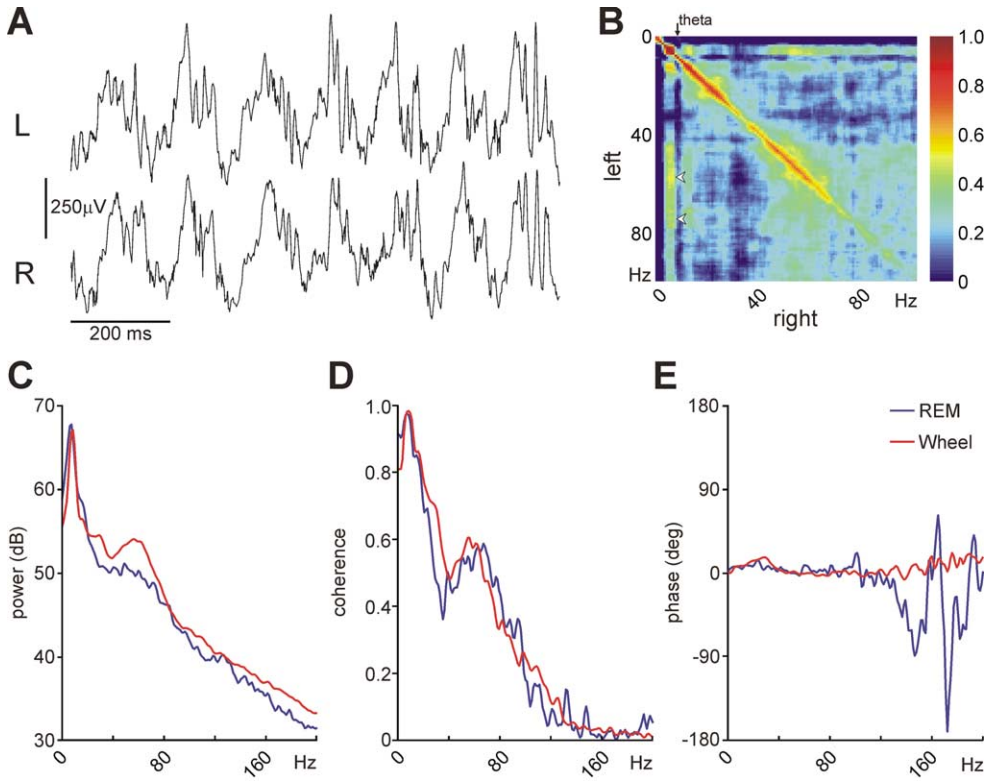

Fig. 5. Bilateral coherence of theta and gamma oscillations. (A) Wire tetrode recordings from the left (L) and right (R) CA1 pyramidal cell layer. (B) Co-modulation of theta and gamma power in the two hemispheres. Note strong co-modulation of theta power, its harmonics and gamma power (diagonal). Note also that theta power in one hemisphere is co-modulated with gamma power of the other hemisphere (yellow band at 9 Hz and 50–100 Hz, white arrowheads). (C) Spectral power of EEG (log scale) recorded from the left hippocampus during wheel running (red) and REM sleep (blue). (D) Coherence spectra between signals derived from the L and R hippocampi. Note high peak at theta-frequency and gamma-frequency band (40–100 Hz) and insignificant coherence in the ripple-frequency band (i.e. >100 Hz). (E) Phase spectra of signals derived from the L and R hippocampi. Note similar phase between 0 and 100 Hz. Phase above 100 Hz is not interpretable, given the very low coherence (see part D). All recordings from the same mouse.

2002). These peaks were not observable in the group average because of the variability of slow rhythms in different mice.

Ripple episodes occurred simultaneously in the left and right CA1 regions, as shown by the co-modulation of ripple power in the two hemispheres (Fig. 6D). However, in contrast to the bilaterally coordinated theta and gamma oscillations, no consistent phase relationship of ripple oscillations was seen between the two hippocampi (Fig. 6A, B), as shown quantitatively by the low coherence values in the ripple frequency band (Fig. 5D). These findings suggest that ripples emerge locally and independently in the two hemispheres (Buzsáki et al., 1992).

Both pyramidal cells and interneurons increased their discharge probability during ripples (Fig. 7A) relative to the baseline period (Csicsvari et al., 1999a,b). Isolated pyramidal cells and multiple unit activity peaked at the peak of the ripple events. As described in the rat (Csicsvari et al., 1999a,b), the ripple event-triggered spike histogram of interneurons had two peaks, one preceding the peak of the ripple event and a second peak 25 ms after the first (Fig. 7A). This distribution was not an artifact of averaging histograms with early and late peaks, because several individual interneurons had bimodal peaks.

Phase locking of neurons to the individual ripple cycles was determined the same way as in the analysis of theta oscillation. The maximum probability of pyramidal cell discharge occurred during the troughs of the field ripple (Fig. 7B). Ripple-phase modulation varied substantially across pyramidal cells, from no reliable phase relationship to very precise time locking. The preferred phase of discharge for the interneuron group was ~30° after the negative peak, corresponding to <1-ms delay between peak activity of the pyramidal cells and interneurons.

Field patterns in the dentate area

As in the CA1 region, two major oscillatory patterns, theta and gamma, were present in the dentate gyrus during exploration and REM sleep, with largest power in the hilus. The presence of theta activity in the dentate hilar region was often less impressive because of the large gamma power in this region (Fig. 1B). Nevertheless, clear theta and gamma peaks were present in the power spectra of hilar recordings (Fig. 8A). The phase difference between theta waves recorded in the CA1 pyramidal layer and hilar region of the dentate gyrus varied from 180 to 270° (inset in Fig. 8C) and the two signals were coherent (Fig. 8C;

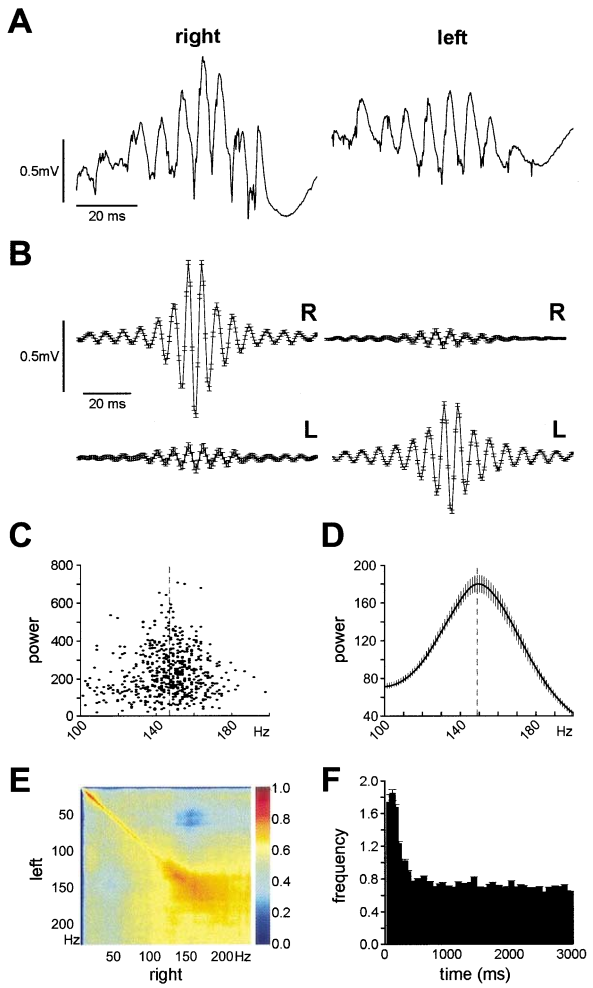

Fig. 6. Interhemispheric relationship of ripples. (A) Simultaneously recorded ripple episodes in the right and left CA1 pyramidal cell layer during slow-wave sleep. (B) Averaged ripples in both sides using the troughs of ripple waves in the right hippocampus (left panel; mean±S.E.) or the left hippocampus (right panel) as reference. Note lack of wave-by-wave relationship between the two hemispheres. (C) Relationship between power and frequency of ripple episodes. Each dot represents a single ripple episode. Vertical line: grand mean ripple frequency. Data from a single mouse. (D) Averaged power (dB) in the 100–200-Hz band (log scale; $n=14$ mice), based on >8 min of continuous recordings during immobility/sleep epochs. (E) Co-modulation of broad high-frequency power in the left and right hippocampus during sleep (100 and 200 Hz). Note largest values at 150 Hz. (F) Inter-ripple histogram. Note peak at 100 ms, indicating frequent occurrence of ripple "doublets."

$n=3$). As in the CA1 region, the power of dentate gamma was also phase-locked to the local theta. The largest gamma power occurred 20–30° after the trough of the local theta (Fig. 8B), i.e. power of gamma oscillation within the theta cycle varied similarly in the CA1 and dentate regions.

During immobility and slow-wave sleep, large-amplitude positive spikes of 10–40-ms duration, termed *dentate field spikes* (DS; Bragin et al., 1995b), were present in the granule cell layer and the hilar region of the dentate gyrus. Unit activity of putative interneurons and principal cells increased several-fold during dentate field spikes (DS) (Fig. 8D). DS occurred synchronously in the two hemispheres.

DISCUSSION

We examined behavior-dependent population patterns in the mouse hippocampus. The phase of theta gradually changed below the CA1 pyramidal layer and reached a maximum amplitude at the level of hippocampal fissure. Theta and gamma waves were highly coherent in the two hemispheres. Sharp wave-associated ripple events occurred simultaneously in the left and right CA1 regions; however, the individual ripple waves were not correlated. Action potentials of CA1 pyramidal cells and interneurons were phase-locked to local theta and gamma oscillations as well as to ripple events. These findings are similar to previous observations in the rat. A major difference between the two species was the larger amplitude of theta, gamma and ripple waves in the mouse. Novel observations included the co-modulation of theta and gamma power and gamma power fluctuation in the CA1 region by the theta cycle.

Theta and gamma oscillations

During exploration and REM sleep, two discrete field rhythms were observed: theta and gamma oscillations. These rhythms were reflected by the bimodal power peaks in spectral histograms. The large peak at theta frequency (6–9 Hz) and its harmonics were clearly separated from the broad gamma power at 40–90 Hz. The distinctness of these bands is further illustrated by the increased coherence values in these frequency bands both within and across hemispheres. Because only these oscillatory patterns are present in the intact hippocampus, oscillations observed in other frequency bands (e.g. beta), reported in *in vitro* preparations (Bland and Oddie, 2001; Bibbig et al., 2001; Bracci et al., 2001; Shimono et al., 2000; Haenschel et al., 2000), may reflect phenomena specific to these particular experimental conditions.

The depth distribution of theta and gamma waves in the CA1 region was similar to that reported in the rat (Winson, 1974; Buzsáki et al., 1983, 1987; Brankack et al., 1993; Bragin et al., 1995a). The gradual phase reversal of theta cycles between CA1 stratum oriens and the hippocampal fissure is consistent with the coordinated activity of multiple current generators (Buzsáki, 2002). Because the largest-amplitude theta waves are observed at the hippocampal fissure, rhythmic excitation of the distal dendrites by the entorhinal afferents are believed to play the most important role in the current generation of extracellular theta (Holsheimer et al., 1982; Buzsáki et al.,. 1983, 1987; Leung, 1984a,b; Brankack et al., 1993). A second theta dipole in the pyramidal layer is assumed to be generated by somatic inhibitory postsynaptic potentials, brought about by the gamma-frequency discharge of basket and chandelier cells, repeated at theta frequency (Artemenko, 1972; Fox, 1989; Leung and Yim, 1986; Ylinen et al., 1995a,b; Kamondi et al., 1998). The similar theta

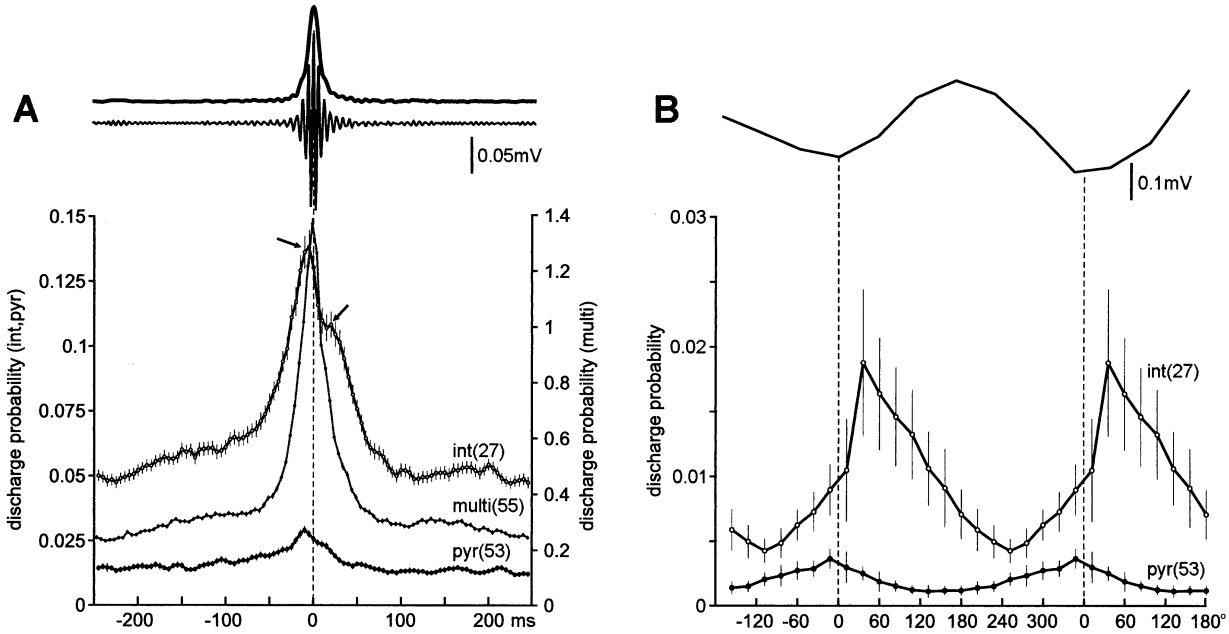

Fig. 7. Ripple modulation of unit activity. (A) Averaged field ripple wave (thin line; 80–250 Hz) and integrated, squared sum of the ripple event (thick line). Discharge probabilities (±S.E.) of pyramidal cells (pyr), interneurons (int) and multiple unit activity (multi) were aligned to the peak of the integrated ripple event (time 0). Arrows, early and late peaks of interneuron discharge. (B) Ripple cycle modulation of pyr and int. Averaged field ripple wave (two cycles shown). Note that interneurons follow pyramidal cells by ~30° (<1 ms for a 150–200-Hz ripple).

phase relationship of the maximum interneuron discharge and gamma power in the mouse lends further support for this suggestion. Finally, the theta phase-locked discharge of CA3 pyramidal neurons ("intrinsic" theta generator; Konopacki et al., 1987) provides another excitatory dipole in the CA1 stratum radiatum (Kocsis et al., 1999).

We found a positive correlation between the magnitude of theta and gamma power. Although gamma patterns can occur in the absence of theta oscillation (Buzsáki et al., 1983, 1987; Leung 1998; Fisahn et al., 1998), these findings suggest that generation of theta and gamma waves shares similar mechanisms. The major inputs responsible for gamma waves in the CA1 area are the CA3 region (Bragin et al., 1995a; Leung, 1998; Csicsvari et al., 1999b), somatic inhibition by basket neurons (Wang and Buzsáki, 1996; Penttonen et al., 1998; Fisahn et al., 1998) and the entorhinal cortex (Charpak et al., 1995). These inputs are precisely the ones involved in the current generation of theta waves as well. The robust relationship between theta and gamma oscillations observed here suggests that gamma frequency discharge of the excitatory and inhibitory inputs is modulated by the slower theta and the coordinated relationship between these two oscillations is responsible for the unique voltage vs. depth profile of theta and gamma waves. Furthermore, these respective oscillations were coupled interhemispherically. Given the relatively weak crossed perforant path (Steward, 1976) and the strong ventral hippocampal commissural system in rodents (Buzsáki and Eidelberg, 1982; Li et al., 1994), these observations suggest an important role of the CA3 system in the coordination of these rhythms.

Both interneurons and pyramidal cells were phase-locked to theta field oscillations. CA1 pyramidal neurons discharged after the trough of the local theta waves, whereas maximum discharge of the combined interneuronal population occurred approximately 60–120° prior to the trough. The phase separation of pyramidal cells and interneurons is somewhat larger than observed in the rat (Fox et al., 1986; Skaggs et al., 1996; Csicsvari et al., 1999a,b). The increased discharge of the interneuron population and the peak power of gamma oscillation occurred on the same phase of theta. These observations support the suggestion that interneuron activity is critical for the generation of physiological gamma patterns (Whittington et al., 1995; Wang and Buzsáki, 1998).

Sharp waves and ripples

In the immobile awake and sleeping animal, theta waves are absent but the CA3 recurrent collateral system sustains perpetual oscillations in the gamma ripple-frequency range (Csicsvari et al., 1999b, 2000). The coordinated discharge of CA3 pyramidal cells depolarizes CA1 pyramidal cells and interneurons, the result of which is a sharp wave in stratum radiatum and a short-lived oscillatory pattern (ripple) in the pyramidal cell layer (Buzsáki et al., 1983, 1992; Ylinen et al., 1995b; Bragin et al., 1999; Csicsvari et al., 2000). That ripple generation is distinct from the mechanisms involved in gamma oscillations (Buzsáki et al., 1983; Csicsvari et al., 1999b; Bibbig et al., 2001) is further supported by the observation that ripple power was least correlated with power in the gamma frequency band.

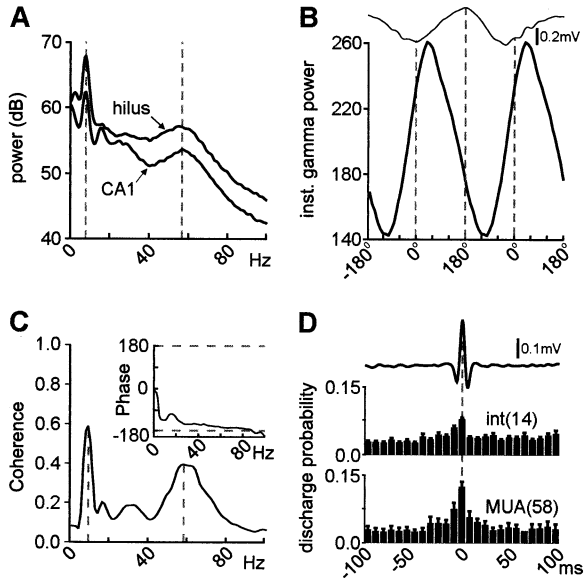

Fig. 8. Field patterns in the dentate hilus. (A) Power spectra of field activity (log scale) recorded from the CA1 pyramidal cell layer and hilus. Note larger power of both theta and gamma oscillations in the hilus. (B) Theta phase modulation of gamma power. (C) Coherence spectrum between the two recording sites in A. Inset: phase spectrum, showing phase reversal of both theta and gamma waves between signals derived from CA1 pyramidal cell layer and hilus. (D) DS and associated unit discharge during non-theta-associated behaviors. Upper trace: average field (reference events: $<$7 S.D. of baseline-filtered [50–150-Hz] field). Cross-correlograms (mean$\pm$S.E.) of isolated interneurons (int) and multiple unit activity (MUA) from all recordings indicate increased unit activity associated with DS.

Ripples in the mouse were also confined to the CA1 pyramidal cell layer. Ripple episodes were associated with a large increase of synchrony of both pyramidal cells and interneurons (McHugh et al., 1996). Previous work has shown that ripple events occurred synchronously along the long axis of the hippocampus and in various parahippocampal structures (Chrobak and Buzsáki, 1996; Csicsvari et al., 2000). Ripple events occurred synchronously in the two hemispheres, as shown by the significant comodulation of ripple power. However, the lack of coherence between individual ripple waves recorded in the two hemispheres supports the view that ripples emerge locally and timing of the pyramidal cells is not coordinated by the afferents that bring about the sharp wave/ripple episode.

Network patterns in the dentate gyrus

Similar to the rat (Vanderwolf, 1969; Buzsáki et al., 1983; Bragin et al., 1995a,b), two antagonistic patterns dominate the dentate gyrus: theta/gamma oscillations and irregular spikelike events. During exploration and REM sleep, large-amplitude gamma waves are present that often obscure ongoing theta waves. Furthermore, power of gamma in the dentate gyrus was phase-locked to the theta cycle as well (Bragin et al., 1995a). Theta waves in the dentate gyrus and CA1 pyramidal cell layer are highly coherent, whereas the mean coherence of gamma waves in the two anatomical regions was relatively low.

Theta activity is absent in the dentate hilus during immobility and sleep. In the absence of theta, gamma oscillation epochs are short and intermittent. Occasionally, a cycle within a short gamma "burst" exceeds the background amplitude several times and these large field events are referred to as dentate spikes (Bragin et al., 1995b). Dentate spikes are associated with synchronous discharge of granule cells and hilar neurons and are believed to be triggered by the entorhinal input (Paré et al., 1995).

Network hippocampal patterns in the mouse and rat are generated by similar mechanisms

A main conclusion of the present work is that the macroscopic physiological patterns in the mouse hippocampus are qualitatively similar to those of the rat. This suggests that the physiological mechanisms that give rise to these patterns are similar in the two species. This conclusion is based on the similar spatial and regional distribution of extracellular voltage changes, bands of oscillation frequencies, the relationship between field and unit activity and the correlation between ongoing local field activity and behavior. A notable difference between the two species is the notably larger amplitude extracellular field (voltage) in the mouse compared with the rat. This was true particularly for high-frequency patterns. Ripple amplitudes could exceed 1 mV in the mouse, an almost two-fold increase relative to that observed in the rat (Ylinen et al., 1995a,b; Csicsvari et al., 1999a,b). Gamma amplitude in the CA1 pyramidal cell layer was several hundred microvolts, whereas in the rat it is hardly recognizable visually in this layer (Bragin et al., 1995a). Theta activity in the CA1 pyramidal cell layer exceeded 0.3 mV in the mouse compared with $<$0.3 mV in the rat (Buzsáki et al., 1983, 1986; Brankack et al., 1993; Bragin et al., 1995a).

Since all observed field patterns had larger amplitude in the mouse, a likely explanation for this difference is the larger "packing density" of neuronal elements in the mouse because of the smaller volume of neurons (Insausti, 1993). In rodents, the width of the pyramidal cell layer corresponds to 2 to 4 times the diameter of pyramidal neurons, whereas in cats, dogs and primates, scattering of pyramidal cells results in a much wider pyramidal cell layer (Insausti, 1993). Comparison of the magnitude of hippocampal field potentials in various species shows progressively diminishing amplitudes from rodents to primates (Winson, 1972; Robinson, 1980). Within-species variability also likely exists (Franke et al., 2001). Given the large inter-strain variations in cell numbers, connectivity and other variables in the limbic system (Girgis, 1970), it is expected that quantitative aspects of the various field patterns described here will vary in different strains of mice. The normative data presented here can serve as a baseline for future experiments on genetically altered mice.

Acknowledgements—This work was supported by NIH (NS34994, MH54671, 1P41RR09754). We thank J. Hetke and K. Wise for supplying us silicon probes.

REFERENCES

Alonso A, Llinás RR (1989) Subthreshold Na+-dependent theta-like rhythmicity in stellate cells of entorhinal cortex layer II. Nature 342:175–177.

Artemenko DP (1972) Role of hippocampal neurons in theta-wave generation. Neurophysioligia 4:409–415.

Bibbig A, Faulkner HJ, Whittington MA, Traub RD (2001) Self-organized synaptic plasticity contributes to the shaping of gamma and beta oscillations in vitro. J Neurosci 21:9053–9067.

Bland BH, Oddie SD (2001) Theta band oscillation and synchrony in the hippocampal formation and associated structures: the case for its role in sensorimotor integration. Behav Brain Res 127:119–136.

Bracci E, Vreugdenhil M, Hack SP, Jefferys JG (2001) Dynamic modulation of excitation and inhibition during stimulation at gamma and beta frequencies in the CA1 hippocampal region. J Neurophysiol 85:2412–2422.

Bragin A, Jando G, Nadasdy Z, Hetke J, Wise K, Buzsáki G (1995a) Gamma (40–100 Hz) oscillation in the hippocampus of the behaving rat. J Neurosci 15:47–60.

Bragin A, Jando G, Nadasdy Z, van Landeghem M, Buzsáki G (1995b) Dentate EEG spikes and associated interneuronal population bursts in the hippocampal hilar region of the rat. J Neurophysiol 73:1691–1705.

Bragin A, Engel J Jr, Wilson CL, Fried I, Buzsáki G (1999) High frequency oscillations in human brain. Hippocampus 9:137–142.

Brankack J, Stewart M, Fox SE (1993) Current source density analysis of the hippocampal theta rhythm: associated sustained potentials and candidate synaptic generators. Brain Res 615:310–327.

Buzsáki G, Eidelberg E (1982) Convergence of associational and commissural pathways on CA1 pyramidal cells of the rat hippocampus. Brain Res 237:283–295.

Buzsáki G, Leung LW, Vanderwolf CH (1983) Cellular bases of hippocampal EEG in the behaving rat. Brain Res 287:139–171.

Buzsáki G, Czopf J, Kondakor I, Kellenyi L (1986) Laminar distribution of hippocampal rhythmic slow activity (RSA) in the behaving rat: current-source density analysis, effects of urethane and atropine. Brain Res 365:125–137.

Buzsáki G, Horvath Z, Urioste R, Hetke J, Wise K (1992) High-frequency network oscillation in the hippocampus. Science 256: 1025–1027.

Buzsáki G (2002) Theta oscillations in the hippocampus. Neuron 33:325–340.

Buzsáki G, Bragin A, Chrobak JJ, Nadasdy Z, Sik A, Hsu M, Ylinen A (1994) Oscillatory and intermittent synchrony in the hippocampus: relevance to memory trace formation. In: Temporal coding in the brain (Buzsáki G, Llinas RR, Singer A, Berthoz W, Christen Y, eds), pp 145–172. Heidelberg: Springer.

Charpak S, Pare D, Llinás R (1995) The entorhinal cortex entrains fast CA1 hippocampal oscillations in the anaesthetized guinea-pig: role of the monosynaptic component of the perforant path. Eur J Neurosci 7:1548–1557.

Chrobak JJ, Buzsáki G (1996) High-frequency oscillations in the output networks of the hippocampal-entorhinal axis of the freely behaving rat. J Neurosci 16:3056–3066.

Csicsvari J, Hirase H, Czurko A, Mamiya A, Buzsáki G (1999a) Fast network oscillations in the hippocampal CA1 region of the behaving rat. J Neurosci 19:RC20.

Csicsvari J, Hirase H, Czurko A, Mamiya A, Buzsáki G (1999b) Oscillatory coupling of hippocampal pyramidal cells and interneurons in the behaving rat. J Neurosci 19:274–287.

Csicsvari J, Hirase H, Mamiya A, Buzsáki G (2000) Ensemble patterns of hippocampal CA3-CA1 neurons during sharp wave-associated population events. Neuron 28:585–594.

Czurkó A, Hirase H, Csicsvari J, Buzsáki G (1999) Sustained activation of hippocampal pyramidal cells by "space clamping" in a running wheel. Eur J Neurosci 11:344–352.

Destrade C (1982) Two types of diencephalically driven RSA (theta) as a means of studying memory formation in mice. Brain Res 234: 486–493.

Fisahn A, Pike FG, Buhl EH, Paulsen O (1998) Cholinergic induction of network oscillations at 40 Hz in the hippocampus in vitro. Nature 394:186–189.

Fox SE, Wolfson S, Ranck JB Jr (1986) Hippocampal theta rhythm and the firing of neurons in walking and urethane anesthetized rats. Exp Brain Res 62:495–508.

Fox SE (1989) Membrane potential and impedance changes in hippocampal pyramidal cells during theta rhythm. Exp Brain Res 77: 283–294.

Franke P, Chollet D, Tafti M (2001) The homeostatic regulation of sleep need is under genetic control. J Neurosci 21:2610–2621.

Girgis M (1970) The rhinencephalon. Acta Anat (Basel) 76:157–199.

Grastyán E, Lissák K, Madarász I, Donhoffer H (1959) Hippocampal electrical activity during the development of conditioned reflexes. Electroencephalogr Clin Neurophysiol 11:409–430.

Gray CM, Maldonado PE, Wilson M, McNaughton B (1995) Tetrodes markedly improve the reliability and yield of multiple single-unit isolation from multi-unit recordings in cat striate cortex. J Neurosci Methods 63:43–54.

Haenschel C, Baldeweg T, Croft RJ, Whittington M, Gruzelier J (2000) Gamma and beta frequency oscillations in response to novel auditory stimuli: a comparison of human electroencephalogram (EEG) data with in vitro models. Proc Natl Acad Sci USA 97:7645–7650.

Hajdu I, Obal F Jr, Fang J, Krueger JM, Rollo CD (2002) Sleep of transgenic mice producing excess rat growth hormone. Am J Physiol Regul Integr Comp Physiol 282:R70–R76.

Harris KD, Henze DA, Csicsvari J, Hirase H, Buzsáki G (2000) Accuracy of tetrode spike separation as determined by simultaneous intracellular and extracellular measurements. J Neurophysiol 84: 401–414.

Harris KD, Henze DA, Hirase H, Leinekugel X, Dragoi G, Czurkó A, Buzsáki G (2002) Spike train dynamics predicts theta-related phase precession in hippocampal pyramidal cells. Nature 417:738–741.

Holsheimer J, Boer J, Lopes da Silva FH, van Rotterdam A (1982) The double dipole model of theta rhythm generation: simulation of laminar field potential profiles in dorsal hippocampus of the rat. Brain Res 235:31–50.

Ikonen S, Tanila H (2001) Effects of metrifonate on the hippocampal theta rhythm of freely moving intact and MS-lesioned mice. Pharmacol Biochem Behav 69:165–172.

Insausti R (1993) Comparative anatomy of the entorhinal cortex and hippocampus in mammals. Hippocampus 3 Spec No19–26.

Jaffard R, Jeantet Y (1981) Posttraining changes in excitability of the commissural path-CA1 pyramidal cell synapse in the hippocampus of mice. Brain Res 220:167–172.

Jefferys JG, Traub RD, Whittington MA (1996) Neuronal networks for induced '40 Hz' rhythms. Trends Neurosci 19:202–208.

Joho RH, Ho CS, Marks GA (1999) Increased gamma- and decreased delta-oscillations in a mouse deficient for a potassium channel expressed in fast-spiking interneurons. J Neurophysiol 82:1855–1864.

Jouvet M (1969) Biogenic amines and the states of sleep. Science 163:32–41.

Kamondi A, Acsady L, Wang XJ, Buzsáki G (1998) Theta oscillations in somata and dendrites of hippocampal pyramidal cells in vivo: activity-dependent phase-precession of action potentials. Hippocampus 8:244–261.

Kasamo K, Murashima YL, Ozawa N, Nakamoto Y, Suzuki J (1992) Simultaneous recordings of electroencephalograms and multiunit activities in the hippocampus during epileptic seizures of E1 mice. Jpn J Psychiatry Neurol 46:523–525.

Kim D, Song I, Keum S, Lee T, Jeong MJ, Kim SS, McEnery MW, Shin S (2001) Lack of the burst firing of thalamocortical relay neurons and resistance to absence seizures in mice lacking alpha(1G) T-type Ca(2+) channels. Neuron 31:35–45.

Kocsis B, Bragin A, Buzsáki G (1999) Interdependence of multiple

theta generators in the hippocampus: a partial coherence analysis. J Neurosci 19:6200–6212.
Konopacki J, MacIver MB, Bland BH, Roth SH (1987) Theta in hippocampal slices: relation to synaptic responses of dentate neurons. Brain Res Bull 18:25–27.
Leinekugel X, Khazipov R, Cannon R, Hirase H, Ben-Ari Y, Buzsáki G (2002) Correlated burst activity in the neonatal hippocampus in vivo. Science 296:2050–2052.
Leung LS (1984a) Theta rhythm during REM sleep and waking: correlations between power, phase and frequency. Electroencephalogr Clin Neurophysiol 58:553–564.
Leung LS (1998) Generation of theta and gamma rhythms in the hippocampus. Neurosci Biobehav Rev 22:275–290.
Leung LS, Yim CY (1986) Intracellular records of theta rhythm in hippocampal CA1 cells of the rat. Brain Res 367:323–327.
Leung LW (1984b) Model of gradual phase shift of theta rhythm in the rat. J Neurophysiol 52:1051–1065.
Leung LW, Yim CY (1991) Intrinsic membrane potential oscillations in hippocampal neurons in vitro. Brain Res 553:261–274.
Li XG, Somogyi P, Ylinen A, Buzsáki G (1994) The hippocampal CA3 network: an in vivo intracellular labeling study. J Comp Neurol 339:181–208.
Llinás RR (1988) The intrinsic electrophysiological properties of mammalian neurons: insights into central nervous system function. Science 242:1654–1664.
McHugh TJ, Blum KI, Tsien JZ, Tonegawa S, Wilson MA (1996) Impaired hippocampal representation of space in CA1-specific NMDAR1 knockout mice. Cell 87:1339–1349.
Noebels JL (1996) Targeting epilepsy genes. Neuron 16:241–244.
O'Keefe J, Nadel L (1978) The hippocampus as a cognitive map. Oxford, Clarendon.
Paré D, Dong J, Gaudreau H (1995) Amygdalo-entorhinal relations and their reflection in the hippocampal formation: generation of sharp sleep potentials. J Neurosci 15:2482–2503.
Penttonen M, Kamondi A, Acsady L, Buzsáki G (1998) Gamma frequency oscillation in the hippocampus of the rat: intracellular analysis in vivo. Eur J Neurosci 10:718–728.
Penttonen M, Nurminen N, Miettinen R, Sirivio J, Henze DA, Csicsvari J, Buzsáki G (1999) Ultra-slow oscillation (0.025 Hz) triggers hippocampal afterdischarges in Wistar rats. Neuroscience 94:735–743.
Pike FG, Goddard RS, Suckling JM, Ganter P, Kasthuri N, Paulsen O (2000) Distinct frequency preferences of different types of rat hippocampal neurones in response to oscillatory input currents. J Physiol 529:205–213.
Robinson TE (1980) Hippocampal rhythmic slow activity (RSA; theta): a critical analysis of selected studies and discussion of possible species-differences. Brain Res 203:69–101.
Rotenberg A, Mayford M, Hawkins RD, Kandel ER, Muller RU (1996) Mice expressing activated CaMKII lack low frequency LTP and do not form stable place cells in the CA1 region of the hippocampus. Cell 87:1351–1361.
Shimono K, Brucher F, Granger R, Lynch G, Taketani M (2000) Origins and distribution of cholinergically induced beta rhythms in hippocampal slices. J Neurosci 20:8462–8473.
Skaggs WE, McNaughton BL, Wilson MA, Barnes CA (1996) Theta phase precession in hippocampal neuronal populations and the compression of temporal sequences. Hippocampus 6:149–172.
Steriade M, Nunez A, Amzica F (1993) A novel slow ($<$1 Hz) oscillation of neocortical neurons in vivo: depolarizing and hyperpolarizing components. J Neurosci 13:3252–3265.
Steward O (1976) Topographic organization of the projections from the entorhinal area to the hippocampal formation of the rat. J Comp Neurol 167:285–314.
Stewart M, Fox SE (1990) Do septal neurons pace the hippocampal theta rhythm? Trends Neurosci 13:163–168.
Stowers L, Holy TE, Meister M, Dulac C, Koentges G (2002) Loss of sex discrimination and male-male aggression in mice deficient for TRP2. Science 295:1493–1500.
Stumpf C (1965) Drug action on the electrical activity of the hippocampus. Int Rev Neurobiol 8:77–138.
Toth M, Grimsby J, Buzsáki G, Donovan GP (1995) Epileptic seizures caused by inactivation of a novel gene, jerky, related to centromere binding protein-B in transgenic mice. Nat Genet 11:71–75.
Vanderwolf CH (1969) Hippocampal electrical activity and voluntary movement in the rat. Electroencephalogr Clin Neurophysiol 26: 407–418.
Vertes RP, Kocsis B (1997) Brainstem-diencephalo-septohippocampal systems controlling the theta rhythm of the hippocampus. Neuroscience 81:893–926.
Wang XJ, Buzsáki G (1996) Gamma oscillation by synaptic inhibition in a hippocampal interneuronal network model. J Neurosci 16: 6402–6413.
Whittington MA, Traub RD, Jefferys JG (1995) Synchronized oscillations in interneuron networks driven by metabotropic glutamate receptor activation. Nature 373:612–615.
Wilson MA, Tonegawa S (1997) Synaptic plasticity, place cells and spatial memory: study with second generation knockouts. Trends Neurosci 20:102–106.
Winson J (1972) Interspecies differences in the occurrence of theta. Behav Biol 7:479–487.
Winson J (1974) Patterns of hippocampal theta rhythm in the freely moving rat. Electroencephalogr Clin Neurophysiol 36:291–301.
Ylinen A, Bragin A, Nadasdy Z, Jando G, Szabo I, Sik A, Buzsáki G (1995a) Sharp wave-associated high-frequency oscillation (200 Hz) in the intact hippocampus: network and intracellular mechanisms. J Neurosci 15:30–46.
Ylinen A, Soltesz I, Bragin A, Penttonen M, Sik A, Buzsáki G (1995b) Intracellular correlates of hippocampal theta rhythm in identified pyramidal cells, granule cells, and basket cells. Hippocampus 5:78–90.

(Accepted 3 September 2002)